Comparison of Three Integral Formulations for the 2-D TE Scattering Problem

NADINE JOACHIMOWICZ AND CHRISTIAN PICHOT

Abstract—**Electromagnetic modeling for biomedical applications requires effective numerical methods. At present, one of the most efficient methods used to solve diffraction problems with dissipative dielectric objects is the FFT-CGM (fast-Fourier-transform conjugate gradient method) [1]–[3]. However, in contrast to TM polarization, substantial errors are found [4] when we use it for computing the internal field distribution in the TE polarization case for 2-D objects. We here analyze the source of these errors and show that the modified method, empirically introduced in [4], is not required if correct terms in the integral equation are accounted for. With this aim in mind, we propose another integral formulation using generalized functions and compare it to several formulations available in the literature. Numerical comparisons are carried out for inhomogeneous dissipative cylinders whose electromagnetic parameters are close to those of biological tissues. The solution associated with this integral formulation appears to behave better than the others, in comparison with the exact analytical solutions.**

I. Introduction

THE DEVELOPMENT of many biological applications in electromagnetics, such as microwave imaging and hyperthermia treatment, requires fast and accurate computation of the fields in inhomogeneous lossy dielectrics. Analytical methods exist only for such simple geometries as cylindrical [5] and spherical ones [6], and are mainly used to check the accuracy of numerical solutions.

Scattering by an inhomogeneous lossy dielectric structure can be formulated in terms of an electric field integral equation. Using pulse basis function expansion and point matching [7], the integral equation can be reduced to a system of linear equations. An efficient technique for manipulating the full matrices which result is to apply the conjugate gradient method and fast Fourier transforms. A recent debate [8], [9] on the deficiency of pulse basis functions casts serious doubt on the applicability of this method to realistic biological problems. In particular, significant inaccuracies are observed for cylindrical objects in the TE polarization case and 3-D bounded objects. Borup and coauthors [4] show that extreme care should be exercized when pulse functions are used to expand the unknown field, and they introduce a new method, called the modified high-frequency Hohmann method, based on the following considerations. First, basis functions should fit the boundaries of the object accurately; second, the contributions from cell boundaries for which there is no dielectric discontinuity should not be included. The purpose of our paper is to show that this last modification is not required if we use the appropriate integral formulation. We introduce an integral formulation, using generalized functions, which we compare to several formulations already available [4], [10]. We choose 2-D formulations to test it, because they are less computationally involved than 3-D ones. For all numerical methods presented below, the conjugate gradient technique [11] is used to solve the linear system, and the convolution products that appear at each iteration are computed by means of fast Fourier transforms.

The first approach (denoted here as MGC1) is a 2-D TE version of Livesay and Chen's method developed for the 3-D case [10]. The integral formulation is obtained by applying the differential operators (divergence and gradient) on the Green function. The kernel is calculated by replacing the square cell by a disk with the same area (a volumic cell was replaced by a sphere with the same volume as in Livesay and Chen's paper). It has been suggested by Hagmann *et al.* [15] that better results could be obtained with an integral formulation in which the charge contribution explicitly appears. Because of this, the second method discussed here (denoted as FFT-CGM [4]) is based on such an integral formulation, the kernel being obtained as with MGC1. In the same paper, it was also proposed that the charge term be integrated along the exact boundary of each elementary square cell. With this aim in mind, we then introduce a third method (denoted as MGC2), which differs from the previous ones in the evaluation of the kernel. The spectral decomposition of the Green function is used in order to integrate the tensor along the exact contour of each elementary cell.

Numerical computations have been carried out for homogeneous and two-layer cylinders whose electromagnetic parameters are close to those of biological tissues. The results which we found with MGC1, MGC2, and FFT-CGM are far from exact [5]. For this reason, we develop another method (denoted as MGC3) by using a generalized function formalism, with the kernel calculated as with MGC2.

Manuscript received February 16, 1989; revised July 26, 1989.

The authors are with Equipe electromagnétisme, Laboratoire des Signaux et Systèmes, CNRS-ESE, Plateau de Moulon, F-91192 Gif-sur-Yvette Cedex, France

IEEE Log Number 8932001.

0018-9480/90/0200-0178$01.00 ©1990 IEEE

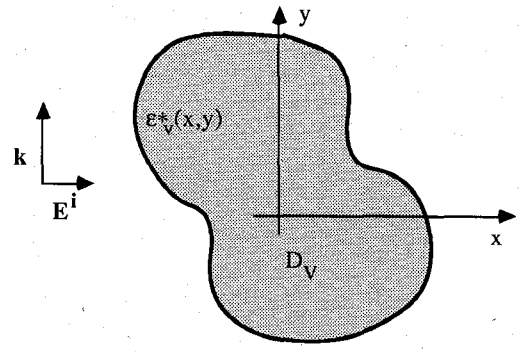

Fig. 1. Geometry of the 2-D TE cylinder.

II. Description of the Methods

Fig. 1 shows an inhomogeneous lossy dielectric cylinder with arbitrarily shaped cross section D_v illuminated by a TE-polarized incident field $\boldsymbol{E}^i$. The total electric field is denoted by $\boldsymbol{E}$. An $\exp(-j\omega t)$ time dependence is implied. It is well known that the scattered field is generated by currents induced inside the object that radiate into the homogeneous exterior region. Let us define the function $\boldsymbol{K}(\boldsymbol{r})$ at point $\boldsymbol{r}$, proportional to induced current $\boldsymbol{J}(\boldsymbol{r})$, as

$$\boldsymbol{K}(\boldsymbol{r}) = \boldsymbol{E}(\boldsymbol{r})(\epsilon_v^*(\boldsymbol{r}) - \epsilon^*) = \boldsymbol{J}(\boldsymbol{r})/j\omega\epsilon_0 \tag{1}$$

where ϵ_v^* and ϵ^* are the complex relative permittivities of the inner and outer regions respectively. $\boldsymbol{E}(\boldsymbol{r})$ is given by

$$\boldsymbol{E}(\boldsymbol{r}) = \boldsymbol{E}^i(\boldsymbol{r}) + (k^2 + 1/\epsilon^* \text{ grad div}) \int_{Dv}\int G(\boldsymbol{r}, \boldsymbol{r}')\boldsymbol{K}(\boldsymbol{r}')\, ds' \tag{2}$$

where $G(\boldsymbol{r}, \boldsymbol{r}')$ is the free-space (the exterior medium) Green's function.

By applying the differential operator grad div on the Green function, we obtain the following integral equation [10], [12]:

$$\begin{aligned}\boldsymbol{E}(\boldsymbol{r}) = \boldsymbol{E}(\boldsymbol{r}) &- k^2 \int_{Dv}\int G(\boldsymbol{r}, \boldsymbol{r}')\boldsymbol{K}(\boldsymbol{r}')\, ds' \\ &- \text{PV} \int\int 1/\epsilon^* \text{ grad}' \text{ div}' G(\boldsymbol{r}, \boldsymbol{r}')\boldsymbol{K}(\boldsymbol{r}')\, ds' \\ &+ 1/(2\epsilon^*)\boldsymbol{K}(\boldsymbol{r})\end{aligned} \tag{3}$$

where PV represents the principal value and grad′ and div′ refer to derivatives with respect to the primed coordinates.

In order to preserve the convolutional form of this integral equation during numerical computation, we apply the method of moments with a pulse basis and point matching. To do so, the object is divided into N elementary square cells with width Δ. It follows that the electric field and the dielectric properties are taken as constant in each cell and that equality is enforced at the cell centers. The resulting linear system is then

$$\begin{aligned}\boldsymbol{E}^i(\boldsymbol{r}_n) = &\left(\frac{\Delta\epsilon^*(\boldsymbol{r}_n)}{2\epsilon^*} + 1\right)\boldsymbol{E}(\boldsymbol{r}_n) \\ &- k^2 \sum_{i=1}^{N} \Delta\epsilon^*(\boldsymbol{r}_i)\boldsymbol{E}(\boldsymbol{r}_i) \int_{S_{\Delta i}}\int G(\boldsymbol{r}_n, \boldsymbol{r}')\, ds' \\ &- \sum_{i=1}^{N} \frac{\Delta\epsilon^*(\boldsymbol{r}_i)}{\epsilon^*}\boldsymbol{E}(\boldsymbol{r}_i) \int_{S_{\Delta i}}\int \text{grad}' \text{ div}' G(\boldsymbol{r}_n, \boldsymbol{r}')\, ds'\end{aligned} \tag{4}$$

where

$$\boldsymbol{r}_n: \begin{pmatrix} x_n \\ y_n \end{pmatrix} \text{ observation point} \qquad \boldsymbol{r}_i: \begin{pmatrix} x_i \\ y_i \end{pmatrix} \text{ source point}$$

$$\Delta\epsilon^*(\boldsymbol{r}_i) = \epsilon_v^*(\boldsymbol{r}_i) - \epsilon^*$$

and $S_{\Delta i}$ is the area of the elementary cell centered at point $\boldsymbol{r}_i$. This relation can be expressed as

$$\begin{aligned}E^i_{xp}(\boldsymbol{r}_n) = T_0(\boldsymbol{r}_n)E_{xp}(\boldsymbol{r}_n) &- k^2 \sum_{i=1}^{N} \mathsf{C}(\boldsymbol{r}_n, \boldsymbol{r}_i)K_{xp}(\boldsymbol{r}_i) \\ &+ \sum_{i=1}^{N}\sum_{q=1}^{2} \Gamma_{xpxq}(\boldsymbol{r}_n, \boldsymbol{r}_i)\frac{K_{xq}(\boldsymbol{r}_i)}{\epsilon^*}\end{aligned} \tag{5}$$

where xp and xq (p and $q = 1, 2$) refer to the x and the y axis respectively and

$$T_0(\boldsymbol{r}_n) = \frac{\Delta\epsilon^*(\boldsymbol{r}_n)}{2\epsilon^*} + 1$$

$$\mathsf{C}(\boldsymbol{r}_n, \boldsymbol{r}_i) = \int_{S_{\Delta i}} G(\boldsymbol{r}_n, \boldsymbol{r}')\, ds'$$

$$\Gamma_{xpxq}(\boldsymbol{r}_n, \boldsymbol{r}_i) = \int_{S_{\Delta i}} \frac{\partial^2}{\partial x'_p \partial x'_q} G(\boldsymbol{r}_n, \boldsymbol{r}')\, ds'.$$

In the first method (MGC1), kernels C and Γ_{xpxq} are calculated analytically by replacing the square cells by disks of equal area [13].

It has been suggested [15] that better results could be obtained with an integral equation in which the charge contribution appears explicitly. Its expression below is deduced from (2):

$$\begin{aligned}\boldsymbol{E}^i(\boldsymbol{r}) = \boldsymbol{E}(\boldsymbol{r}) &- k^2 \int_{Dv}\int G(\boldsymbol{r}, \boldsymbol{r}')\boldsymbol{K}(\boldsymbol{r}')\, ds' \\ &+ \int_{Dv}\int 1/\epsilon^* \text{ grad}' G(\boldsymbol{r}, \boldsymbol{r}') \text{ div}' \boldsymbol{K}(\boldsymbol{r}')\, ds'.\end{aligned} \tag{6}$$

Here, the first integral is associated with the polarization current, and the second with the charge. If we assume that the cross section D_v can be divided into M homogeneous subregions V_m, the divergence of the function $\boldsymbol{K}(\boldsymbol{r})$ in the second integral is nonzero only at the interfaces between subregions. This integral then reduces to a line integral along such interfaces [14], and (6) is given by

$$\begin{aligned}\boldsymbol{E}^i(\boldsymbol{r}) = \boldsymbol{E}(\boldsymbol{r}) &- k^2 \sum_{m=1}^{M} \Delta\epsilon_m^* \cdot \int_{S_m}\int \boldsymbol{E}(\boldsymbol{r}')G(\boldsymbol{r}, \boldsymbol{r}')\, ds' \\ &- \sum_{m=1}^{M} \frac{\Delta\epsilon_m^*}{\epsilon^*} \cdot \int_{C_m} \boldsymbol{E}(\boldsymbol{r}') \cdot \boldsymbol{n}' \text{ grad}' G(\boldsymbol{r}, \boldsymbol{r}')\, dl'\end{aligned} \tag{7}$$

with $\Delta\epsilon_m^* = \epsilon_{vm}^* - \epsilon^*$, where ϵ_{vm}^* is the complex relative permittivity of region V_m. The quantity $\boldsymbol{n}'$ is the outward-directed unit normal vector, S_m is the surface area of region V_m, and C_m is the boundary of region V_m.

By dividing each homogeneous subregion into elementary cells and using the same method of discretization as above, we obtain the linear system

$$\boldsymbol{E}^t(\boldsymbol{r}_n) = \boldsymbol{E}(\boldsymbol{r}_n) - k^2 \sum_{t=1}^{N} \Delta\epsilon^*(\boldsymbol{r}_t)\boldsymbol{E}(\boldsymbol{r}_t) \int_{S_{\Delta t}} \int G(\boldsymbol{r}_n, \boldsymbol{r}')\, ds' - \sum_{t=1}^{N} \frac{\Delta\epsilon^*(\boldsymbol{r}_t)}{\epsilon^*} \boldsymbol{E}(\boldsymbol{r}_t) \int_{C_{\Delta t}} \cdot \boldsymbol{n}' \operatorname{grad}' G(\boldsymbol{r}_n, \boldsymbol{r}')\, dl' \quad (8)$$

where $C_{\Delta t}$ is the boundary of the elementary cell centered at point $\boldsymbol{r}_t$. This relation can be written as

$$E_{xp}^t(\boldsymbol{r}_n) = E_{xp}(\boldsymbol{r}_n) - k^2 \sum_{t=1}^{N} \mathsf{C}(\boldsymbol{r}_n, \boldsymbol{r}_t) K_{xp}(\boldsymbol{r}_t) - \sum_{t=1}^{N} \sum_{q=1}^{2} {}^{+}\mathsf{G}_{xpxq}(\boldsymbol{r}_n, \boldsymbol{r}_t) \frac{\Delta\epsilon^*(\boldsymbol{r}_t)}{\epsilon^*} E_{xq}(\boldsymbol{r}_t) + \sum_{t=1}^{N} \sum_{q=1}^{2} {}^{-}\mathsf{G}_{xpxq}(\boldsymbol{r}_n, \boldsymbol{r}_t) \frac{\Delta\epsilon^*(\boldsymbol{r}_t)}{\epsilon^*} E_{xq}(\boldsymbol{r}_t) \quad (9)$$

with the introduction of

$${}^{+\text{or}-}\mathsf{G}_{xpxq}(\boldsymbol{r}_n, \boldsymbol{r}_t) = \int_{{}^{+\text{or}-}C_{\Delta t}} n_q' \operatorname{grad}'_{xp} G(\boldsymbol{r}_n, \boldsymbol{r}')\, dl'.$$

${}^{+\text{or}-}C_{\Delta t}$ represents the two opposite sides of the elementary cell, orthogonal to the normal $\boldsymbol{n}'$.

The second method (FFT-CGM) is based on the solution (9) with the kernel calculated in the same manner as with MGC1, by replacing the square cell by a disk of equal area. As suggested in [15], the term grad' G could be integrated along the exact boundary of each elementary cell. To test the effect of this modification we introduce method MGC2, which is still based on the solution of (9), but where the contribution of the charge is estimated by using the spectral decomposition of the Green function (plane wave expansion). With this scheme, the transform of G_{xpxq} functions are evaluated analytically, since derivations and integrations of the Green function are converted to multiplication and division factors in the spectral domain. However, since these functions are not band-limited in the spectral domain, it is necessary to zero-pad in order to avoid aliasing and to approximate an infinite domain. Computations have shown that, starting with the analytical spectral expression of G_{xpxq} and using FFT algorithms, a period of at least 30 times the width of the object must be chosen. This requirement is due to the narrow extent of the functions in the spatial domain. In order to reduce storage and computation time for each iteration without sacrificing accuracy, we employ a procedure suggested in [16], as follows:

- The spectral kernel function is Fourier transformed over $30N$ sampling points by using a FFT algorithm.
- The spatial function obtained is then truncated on $2N$ points, which is enough to depict the function correctly. Fourier transforming this truncated function back once again into the spectral domain by using FFT yields the desired approximation for the spectral expressions of G_{xpxq} functions.

This form can be used henceforth for carrying out the convolution operations at each iteration in the conjugate gradient algorithm [3]. Let us note that Hagmann *et al.* [15], using different arguments, have developed a method (HFH) wherein the kernel is also integrated along the exact boundary of the elementary cell. This will allow us to test the method MGC2.

We have compared these different methods to the exact (series of normal modes), as computed in [5]. All numerical results appear to be far from the exact ones, as seen in Section III below. To overcome such a discrepancy, we introduce a new integral formulation by using a generalized function formalism. The derivatives of the discontinuous function $\boldsymbol{K}(\boldsymbol{r})$ must be estimated carefully. The generalized function formalism allows us to take into account such discontinuities and to obtain an integral formulation where the jump σ in the function $1/\epsilon_v^*$ appears at any boundary C of discontinuity (the notations used below are the same as in Rodier [17]).

Thus, div $\boldsymbol{K}$ is written as

$$\operatorname{div} \boldsymbol{K}(\boldsymbol{r}) = \{\operatorname{div} \boldsymbol{K}(\boldsymbol{r})\} + \boldsymbol{n} \cdot \sigma_{\boldsymbol{K}} \delta_C \quad (10)$$

where $\{\ \}$ means that the derivatives are taken in the function sense and δ_C is the cylindrical Dirac function defined on C (line discontinuity of $\epsilon_v^*(\boldsymbol{r})$). From (1) we obtain

$$1/\epsilon^* \operatorname{div} \boldsymbol{K}(\boldsymbol{r}) = 1/\epsilon^* \operatorname{div} \epsilon_v^*(\boldsymbol{r})\boldsymbol{E}(\boldsymbol{r}) - \operatorname{div} \boldsymbol{E}(\boldsymbol{r}). \quad (11)$$

Using the vector identity

$$1/\epsilon_v^*(\boldsymbol{r}) \operatorname{div} (\epsilon_v^*(\boldsymbol{r})\boldsymbol{E}(\boldsymbol{r})) = \operatorname{div} \boldsymbol{E}(\boldsymbol{r}) - \epsilon_v^*(\boldsymbol{r})\boldsymbol{E}(\boldsymbol{r}) \cdot \operatorname{grad} (1/\epsilon_v^*(\boldsymbol{r})) \quad (12)$$

and taking into account that $\operatorname{div}(\epsilon_v^* \boldsymbol{E})$ is zero yields

$$\{\operatorname{div} \boldsymbol{E}(\boldsymbol{r})\} + \boldsymbol{n} \cdot \sigma_{\boldsymbol{E}} \delta_C = \epsilon_v^*(\boldsymbol{r})\boldsymbol{E}(\boldsymbol{r}) \cdot \left(\{\operatorname{grad} (1/\epsilon_v^*(\boldsymbol{r}))\} + \boldsymbol{n}\sigma \frac{1}{\epsilon_v^*} \delta_C \right). \quad (13)$$

Introducing (13) into (6), we obtain the integral equation

$$\boldsymbol{E}^t(\boldsymbol{r}) = \boldsymbol{E}(\boldsymbol{r}) - k^2 \int_{Dv} \int G(\boldsymbol{r}, \boldsymbol{r}')\boldsymbol{K}(\boldsymbol{r}')\, ds' - \int_{Dv} \int \epsilon_v^*(\boldsymbol{r}')\boldsymbol{E}(\boldsymbol{r}') \cdot \{\operatorname{grad}'(1/\epsilon_v^*(\boldsymbol{r}'))\} \cdot \operatorname{grad}' G(\boldsymbol{r}, \boldsymbol{r}')\, ds' - \int_{\Sigma C} \epsilon_v^*(\boldsymbol{r}')\boldsymbol{E}(\boldsymbol{r}') \cdot \boldsymbol{n}' \sigma_{1/\epsilon_v^*}(\boldsymbol{r}') \operatorname{grad}' G(\boldsymbol{r}, \boldsymbol{r}')\, dl' \quad (14)$$

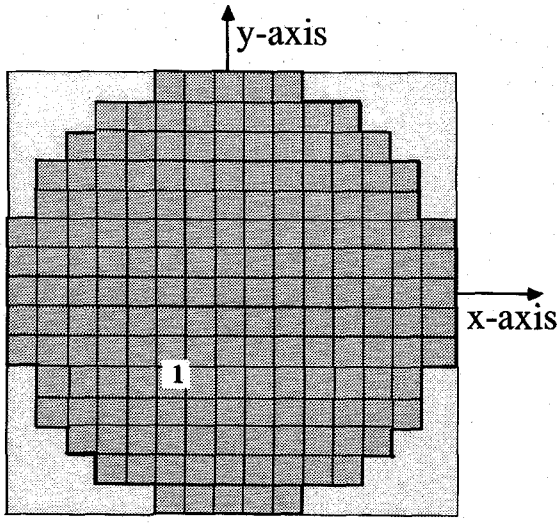

(a)

Fig. 2. (a) Geometry of the homogeneous circular cylinder. Outer layer radius = 15 cm, frequency = 300 MHz; $\epsilon_{rv1} = 54$, $\sigma_{v1} = 1.4$ S/m.

where $\int_{\Sigma C}$ indicates integration along all contours of discontinuity of the function $\epsilon_v^*(\boldsymbol{r})$.

With the integral formulation being discretized in the same way as before, the second integral vanishes since the parameters are constant within the elementary cell; the resulting linear system is

$$\begin{aligned} \boldsymbol{E}^i(\boldsymbol{r}_n) = \boldsymbol{E}(\boldsymbol{r}_n) - k^2 \sum_{i=1}^{N} \Delta\epsilon^*(\boldsymbol{r}_i)\boldsymbol{E}(\boldsymbol{r}_i) \int_{S_{\Delta i}} \int G(\boldsymbol{r}_n, \boldsymbol{r}')\, ds' \\ - \sum_{i=1}^{N} \epsilon_v^*(\boldsymbol{r}_i)\sigma_{1/\epsilon_v^*}(\boldsymbol{r}_i)\boldsymbol{E}(\boldsymbol{r}_i) \\ \cdot \int_{C_{\Delta i}} \cdot \boldsymbol{n}' \operatorname{grad}' G(\boldsymbol{r}_n, \boldsymbol{r}')\, dl' \end{aligned} \tag{15}$$

where $\sigma_{1/\epsilon_v^*}(\boldsymbol{r}_i)$ is the jump in the function $1/\epsilon_v^*$ between two contiguous cells. As in the above, (15) is written

$$\begin{aligned} E_{xp}^i(\boldsymbol{r}_n) = E_{xp}(\boldsymbol{r}_n) - k^2 \sum_{i=1}^{N} \mathsf{C}(\boldsymbol{r}_n, \boldsymbol{r}_i) K_{xp}(\boldsymbol{r}_i) \\ - \sum_{i=1}^{N} \sum_{q=1}^{2} {}^{+}\mathsf{G}_{xpxq}(\boldsymbol{r}_n, \boldsymbol{r}_i) \cdot \epsilon_v^*(\boldsymbol{r}_i) \\ {}^{+}\sigma_{xq,1/\epsilon_v^*}(\boldsymbol{r}_i) E_{xq}(\boldsymbol{r}_i) \\ - \sum_{i=1}^{N} \sum_{q=1}^{2} {}^{-}\mathsf{G}_{xpxq}(\boldsymbol{r}_n, \boldsymbol{r}_i) \epsilon_v^*(\boldsymbol{r}_i) \\ {}^{-}\sigma_{xq,1/\epsilon_v^*}(\boldsymbol{r}_i) E_{xq}(\boldsymbol{r}_i) \end{aligned} \tag{16}$$

with

$$ {}^{\pm}\sigma_{xq,1/\epsilon_v^*}(\boldsymbol{r}_i) = \pm \left[\frac{1}{\epsilon_v^*(x_{i\pm j}, y_{i\pm k})} - \frac{1}{\epsilon_v^*(x_i, y_i)} \right] $$

$$q = 1, \quad xq = x \rightarrow j = 1 \text{ and } k = 0$$

$$q = 2, \quad xq = y \rightarrow j = 0 \text{ and } k = 1.$$

These expressions take into account the orientation of the normal vector (the contiguous cells being defined as (x_i, y_i) and $(x_{i\pm j}, y_{i\pm k})$).

The last method, MGC3, is based on the solution of (16), the associated kernels being computed as with MGC2.

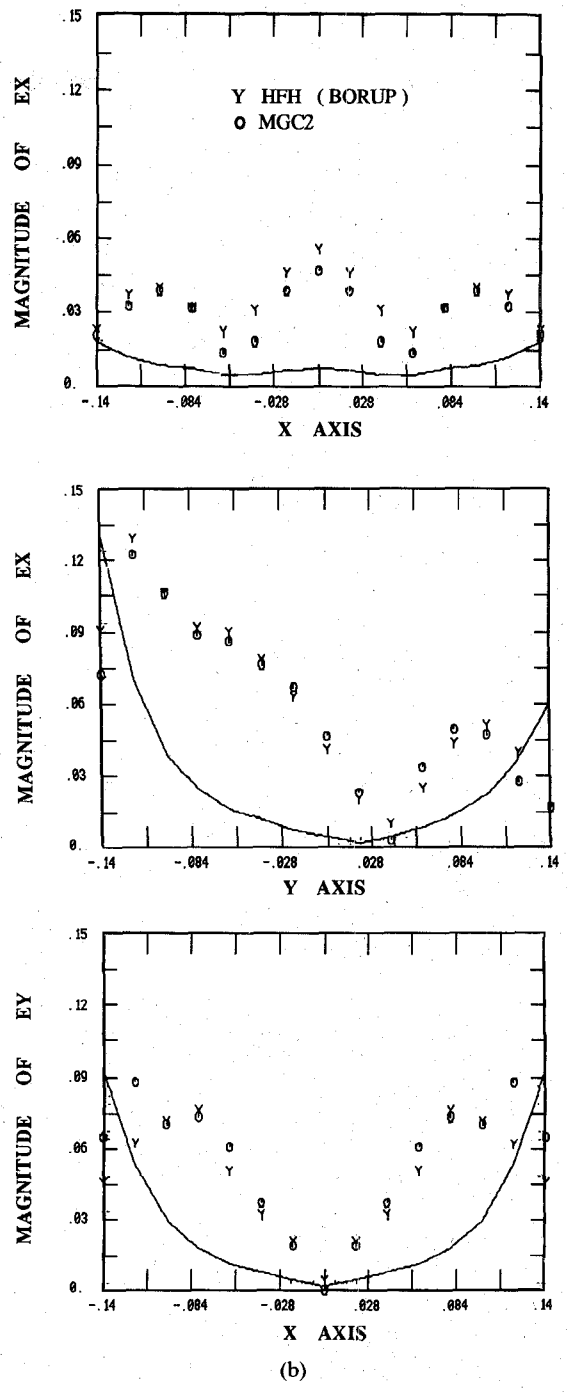

(b)

Fig. 2. (*Continued*) (b) Comparison between HFH and MGC2 solutions versus analytic solution (the electric fields are normalized with respect to E_i).

III. Numerical Results

In order to compare the results obtained by these different methods to those given in [4], we consider the same objects. They are homogeneous and inhomogeneous cylinders (radius = 15 cm), composed of muscle or muscle and fat, which are illuminated at 100 and 300 MHz. They are

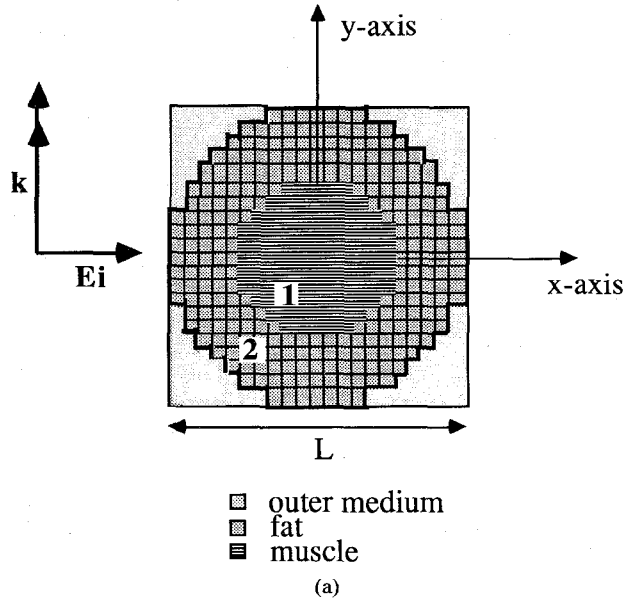

(a)

Fig. 3. (a) Geometry of the layered circular cylinder. Outer layer radius = 15 cm, inner layer radius = 7.9 cm. Frequency = 100 MHz; $\epsilon_{rv1} = 72$, $\epsilon_{rv2} = 7.5$; $\sigma_{v1} = 0.9$ S/m, $\sigma_{v2} = 0.048$ S/m.

enclosed inside a square divided into elementary square cells. All numerical results have been computed by using a conjugate gradient solution method of linear systems. This requires choosing an initial guess of the unknowns and using some criterion to stop the iterative procedure. In each case the incident field is chosen as the initial guess. The process is stopped when the squared norm of the residual vector (which is at the ith iteration $AX_i - Y$ if $AX = Y$ denotes the linear system to be solved), divided by the one of the incident field, falls below 10^{-3}. For every test case presented we display the magnitude of the field component (E_x, E_y), normalized with respect to the incident field. All results are compared with the exact results computed as in [5], which we represent by a solid line.

The first test case is a muscle cylinder ($\epsilon_{rv1} = 54$, $\sigma_{v1} = 1.4$ S/m) divided into 15×15 square cells and illuminated at 300 MHz (Fig. 2(a)). The results obtained with MGC2 are shown in Fig. 2(b) and are compared to those obtained with the HFH method [4]. The results are quite similar, which shows that the procedure used for computing the kernel in MGC2 does not suffer from aliasing. However, severe errors are present in both cases. Fig. 3(a) shows the model used in the next test cases. This is a two-layer cylinder with an inner layer (radius = 15 cm) of muscle ($\epsilon_{rv1} = 72$, $\sigma_{v1} = 0.9$ S/m) and an outer layer (radius = 7.9 cm) of fat ($\epsilon_{rv2} = 7.5$, $\sigma_{v2} = 0.048$ S/m). This object is divided into 21×21 cells and is illuminated at 100 MHz. Fig. 3(b) compares MGC1 and FFT-CGM. The results are almost the same, but there is considerable error on the tangential component of the field at both circular interfaces. Formulations (3) and (7) are proved to be equivalent and so the explicit introduction of the charge term in the integral equation is not satisfactory. Fig. 3(c) compares FFT-CGM and MGC2. The MGC2 results differ slightly

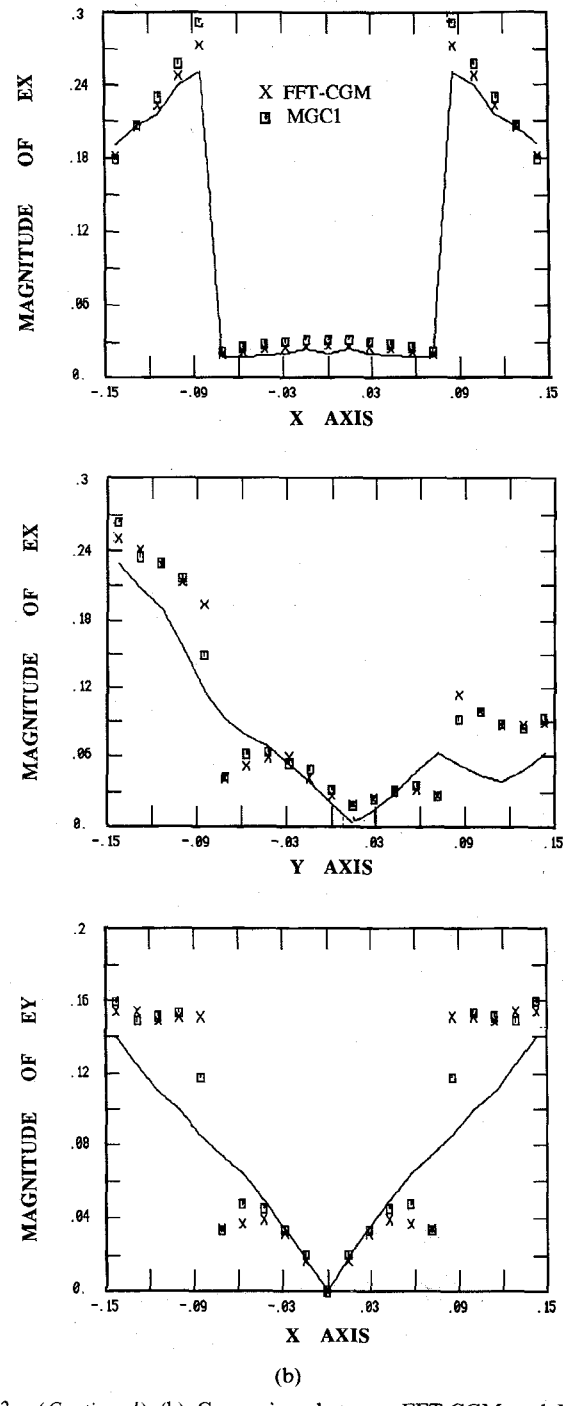

(b)

Fig. 3. (*Continued*) (b) Comparison between FFT-CGM and MGC1 solutions.

from those in Fig. 3(b). Thus we do not benefit from the integration of the kernel along the exact contour of the elementary cell. Two modifications are now suggested in [4] to improve the results. The first one is to divide the object into irregularly shaped cells which better fit the curved boundaries. Indeed, taking into account that the charge contribution in (7) is a line integral, the results must be quite sensitive to the description of this contour. Unfortunately, this modified approach does not allow us to use FFT's and will cost in both storage and computation time. It is clearly not useful if we solve the problem for an object with no curved boundary. The second modi-

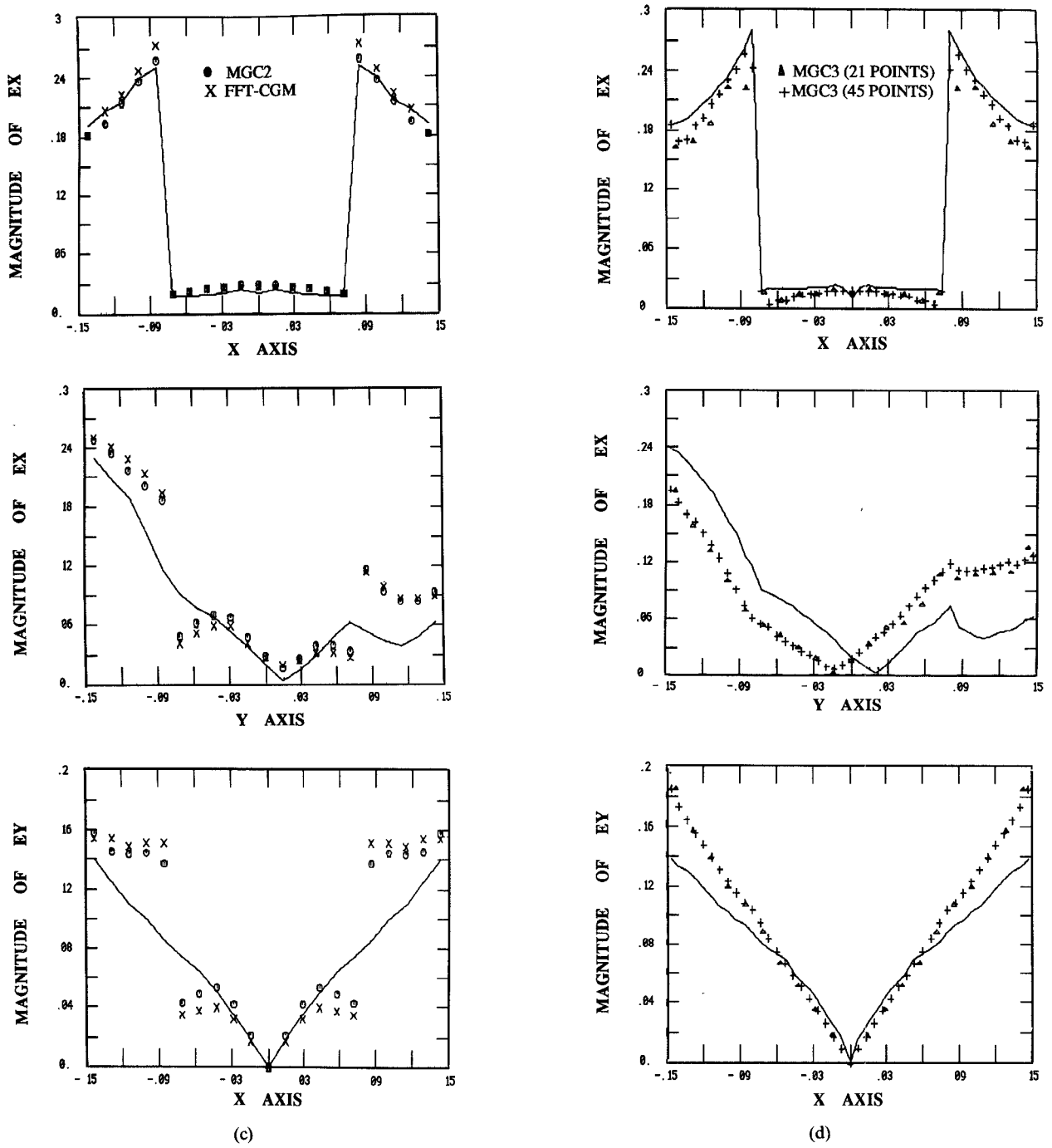

Fig. 3. (*Continued*) (c) Comparison between FFT-CGM and MGC2 solutions. (d) Comparison between MGC3 solutions for two different discretizations.

fication is related to the fact that pulse basis functions introduce fictitious charges in the interior of homogeneous regions. To ignore this deficiency, the contributions from cell boundaries for which there is no actual dielectric discontinuity have to be excluded. We believe that this second modification is not useful if we have the appropriate formulation (14). Fig. 3(d) shows the results obtained with MGC3 for the same object divided into 21×21 and 45×45 square cells. The agreement of the results for the two types of discretization shows that the method is convergent. Furthermore, the results appear quite smooth and are different from the previous ones. Without using the two modifications, the fictitious discontinuities that appear in previous methods for the E_x component along the y axis and for the tangential component disappear. In order to confirm this observation, we have studied a two-layer cylinder with an inner layer (radius = 15 cm) of muscle ($\epsilon_{rv1} = 54$, $\sigma_{v1} = 1.4$ S/m) and an outer layer (radius = 9.4 cm) of fat ($\epsilon_{rv2} = 5.7$, $\sigma_{v2} = 0.05$ S/m), shown in Fig. 4(a). This object is divided into 15×15 cells and illuminated at 300 MHz. Fig. 4(b) compares MGC2 with MGC3. Results show that, in contrast to MGC2, MGC3 predicts the jump discontinuity in E_x along x and as a general rule gives a smoother solution.

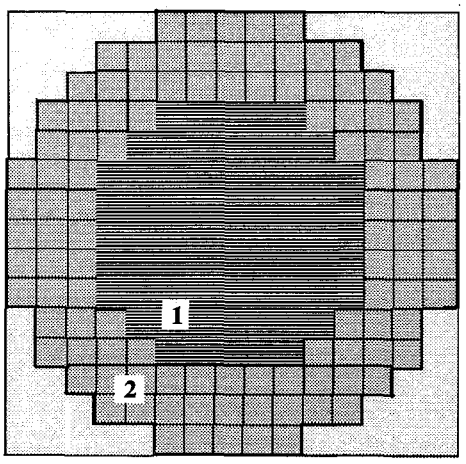

(a)

Fig. 4a. (a) Geometry of the layered circular cylinder. Outer layer radius = 15 cm; inner layer radius = 9.4 cm. Frequency = 300 MHz; $\epsilon_{r1} = 54$, $\epsilon_{r2} = 5.7$; $\sigma_{r1} = 1.4$ S/m, $\sigma_{r2} = 0.05$ S/m.

Note that if we deal with objects for which boundaries are correctly depicted with square cells, the method MGC3 should provide accurate results.

IV. Conclusion

It has been shown that the inclusion of the derivatives in the electric field integral equation for the 2-D TE polarization scattering may cause serious errors when a method of moments with pulse basis and point matching is applied. Current discussions focus on the adequacy of the pulse basis function [4], [8], [9]. An efficient numerical method (fast Fourier transform conjugate gradient method) has been developed [1]–[3] to solve the scattering problem. However, this method is based on the convolutional form of the linear system, which has been preserved by using pulse basis functions in the moment method. In order to use this technique to solve the 2-D TE scattering problem, we have analyzed these errors by comparing several methods which differ from one another by the formulations and the approximations used. It appears that the best results are obtained by means of an integral formulation where generalized functions are used. However, since the test cases are cylinders (for which an analytical solution is known), the results still differ from the exact ones, because of the inadequacy of the pulse basis in fitting curved boundaries. Nevertheless, the method presented here (MGC3) is numerically efficient by using FFT algorithms and could be applied to objects for which boundaries are correctly depicted with square cells.

In summary, the sources of the errors are

- the integral formulation, which must explicitly take into account the discontinuities existing at each boundary (at the surface and inside the object), and
- the line integral, which must be computed along a boundary as close as possible to the real contour.

For these reasons we have proposed an integral formulation that uses generalized functions. Its numerical implementation is simple and does not require an inordinate amount of time or storage (with respect to the convergence of the iterative method). The solution behaves better than others. However, if we wish to deal with objects of revolution with arbitrary cross section, we must employ basis functions that better fit the boundaries. This will be studied in the near future.

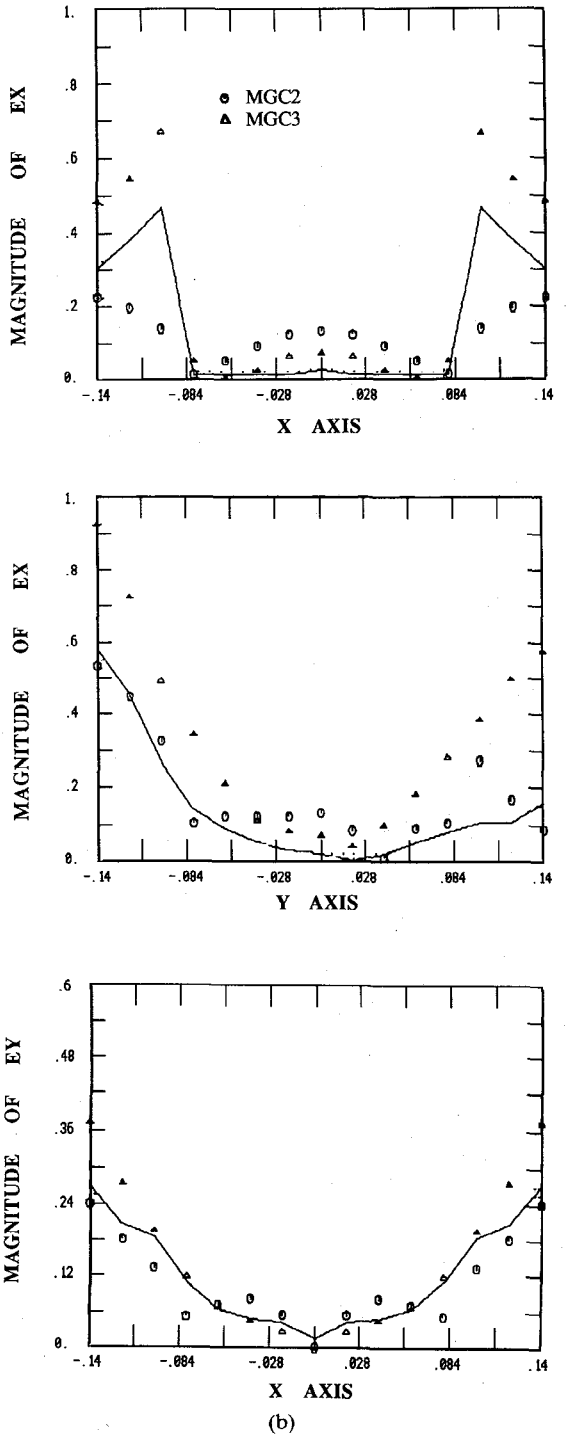

(b)

Fig. 4. (*Continued*) (b) Comparison between MGC3 and MGC2 solutions.

Acknowledgment

The authors are grateful to B. Duchêne and D. Lesselier for helpful discussions and for critically reviewing the manuscript.

REFERENCES

[1] D. Lesselier, d. Vuillet-Laurent, F. Jouvie, and W. Tabbara, "Iterative solution of some direct and inverse problems in electromagnetics and acoustics," *Electromagnetics*, vol. 5, pp. 147–189, 1985.

[2] D. T. Borup and O. P. Ghandhi, "Calculation of high-resolution *SAR* distributions in biological bodies using FFT algorithm and the conjugate gradient method," *IEEE Trans. Microwave Theory Tech.*, vol. MTT-33, pp. 417–419, May 1985.

[3] T. K. Sarkar, E. Arvas, and S. M. Rao, "Application of FFT and the conjugate gradient method for the solution of electromagnetic radiation from electrically large and small conducting bodies," *IEEE Trans. Antennas Propagat.*, vol. AP. 34, pp. 635–640 May 1986.

[4] D. T. Borup, D. M. Sullivan, and O. P. Ghandhi, "Comparison of the FFT conjugate gradient method and the finite-difference time-domain method for the 2-D absorption problem," *IEEE Trans. Microwave Theory Tech.*, vol. MTT-35, pp. 383–395, Apr. 1987.

[5] H. E. Bussey and J. H. Richmond, "Scattering by a lossy dielectric circular cylindrical multilayer, numerical values," *IEEE Trans. Antennas Propagat.*, vol. AP-23, pp. 723–725, Sept. 1975.

[6] J. J. Mikulsi and E. L. Murphy, "The computation of the electromagnetic scattering from concentric spherical structures," *IEEE Trans. Antennas Propagat.*, vol. AP-11, pp. 169–176, Mar. 1963.

[7] R. F. Harrington, *Field Computation by Moment Methods*. New York: Macmillan, 1968.

[8] H. Massoudi, C. H. Durney, and M. F. Iskander, "Limitations of the cubical block model of man in calculating *SAR* distributions," *IEEE Trans. Microwave Theory Tech.*, vol. MTT-32, pp. 746–752, Aug. 1984.

[9] M. J. Hagmann, "Comments on 'Limitations of the cubical block model of man in calculating SAR distributions'," *IEEE Trans. Microwave Theory Tech.*, vol. MTT-33, pp. 347–350, Apr. 1985.

[10] D. E. Livesay and K. M. Chen, "Electromagnetic fields induced inside arbitrarily shaped biological bodies," *IEEE Trans. Microwave Theory Tech.*, vol. MTT-22, pp. 1273–1280, Dec. 1974.

[11] M. Hestenes and E. Stiefel, "Method of conjugate gradients for solving linear systems," *J. Res. Nat. Bur. Stand.*, Sect. B., vol. 49, pp. 409–436, 1952.

[12] C.-C. Su, "A simple evaluation of some principal value integrals for dyadic Green's function using symmetry property," *IEEE Trans. Antennas Propagat.*, vol. AP-35, pp. 1306–1307, Nov. 1987.

[13] J. H. Richmond, "TE-wave scattering by a dielectric cylinder of arbitrary cross section shape," *IEEE Trans. Antennas Propagat.*, vol. AP-14, pp. 460–464, July 1966.

[14] S. C. Hill, C. H. Durney, and D. A. Christensen, "Numerical calculations of low-frequency TE fields in arbitrarily shaped inhomogeneous lossy dielectric cylinders," *Radio Sci.*, vol. 18, pp. 328–336, May–June 1983.

[15] M. J. Hagmann and R. L. Levin, "Convergence of local and average values in three-dimensional moment-method solutions," *IEEE Trans. Microwave Theory Tech.*, vol. MTT-33, pp. 649–654, July 1985.

[16] C. H. Chan and R. Mittra, "Some recent developments in iterative techniques for solving electromagnetic boundary value problems," *Radio Sci.*, vol. 22, pp. 929–934, Nov. 1987.

[17] F. Rodier, *Distributions et transformation de Fourier*, McGraw-Hill, 1988.

Nadine Joachimowicz was born in Paris, France, on December 12, 1963. She received the Maitrise degree in physics and the diplome d'Etudes Approfondies in physical methods for remote sensing from the University of Paris-VII (Jussieu) in 1985 and 1986, respectively. She is currently working toward the Doctorat degree in microwave imaging for biomedical applications. Her fields of interest are direct and inverse problems in electromagnetism.

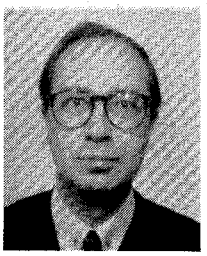

Christian Pichot was born in Rozay-en-Brie, France, in 1951. He received the M.S. degree from the University of Nice, France, in 1974. From the University of Paris-XI (Orsay), France, he received the Doctorat of 3ème Cycle and the Doctorat es Sciences in 1977 and 1982 respectively.

He joined the Equipe Electromagnétisme of the Laboratoire des Signaux et Systèmes in 1978. He is presently a Chargé de Recherche (Staff Research Scientist) at the French Centre National de la Recherche Scientifique (C.N.R.S.). His research activities are concerned with scattering, direct and inverse, and guided wave problems in inhomogeneous media. Since 1981, he has been involved in microwave imaging for biomedical applications and since 1983 for civil engineering applications.

Dr. Pichot received the Microwave Prize of the European Microwave Conference in Nürnberg, West Germany, in 1983.